CVGIP: GRAPHICAL MODELS AND IMAGE PROCESSING
Vol. 56, No. 5, September, pp. 371–391, 1994

Reconstructing Binary Polygonal Objects from Projections: A Statistical View[1]

PEYMAN MILANFAR[2]

SRI International, 333 Ravenswood Avenue, Menlo Park, California 94025

AND

WILLIAM C. KARL AND ALAN S. WILLSKY

Laboratory for Information and Decision Systems, Department of Electrical Engineering and Computer Science, Massachusetts Institute of Technology, Cambridge, Massachusetts 02139

Received August 25, 1993; revised May 11, 1994; accepted May 25, 1994

In many applications of tomography, the fundamental quantities of interest in an image are geometric ones. In these instances, pixel-based signal processing and reconstruction is at best inefficient, and, at worst, nonrobust in its use of the available tomographic data. Classical reconstruction techniques such as filtered back-projection tend to produce spurious features when data is sparse and noisy; these "ghosts" further complicate the process of extracting what is often a limited number of rather simple geometric features. In this paper, we present a framework that, in its most general form, is a statistically optimal technique for the extraction of specific geometric features of objects directly from the noisy projection data. We focus on the tomographic reconstruction of binary polygonal objects from sparse and noisy data. In our setting, the tomographic reconstruction problem is essentially formulated as a (finite-dimensional) parameter estimation problem. In particular, the vertices of binary polygons are used as their defining parameters. Under the assumption that the projection data are corrupted by Gaussian white noise, we use the maximum likelihood (ML) criterion, when the number of parameters is assumed known, and the minimum description length (MDL) criterion for reconstruction when the number of parameters is not known. The resulting optimization problems are nonlinear and thus are plagued by numerous extraneous local extrema, making their solution far from trivial. In particular, proper initialization of any iterative technique is essential for good performance. To this end, we provide a novel method to construct a reliable yet simple initial guess for the solution. This procedure is based on the estimated moments of the object, which may be conveniently obtained directly from the noisy projection data. © 1994 Academic Press, Inc.

[1] This work was supported by the National Science Foundation under Grant 9015281-MIP, the Office of Naval Research under Grant N00014-91-J-1004, the U.S. Army Research Office under Contract DAAL03-92-G-0115, and the Clement Vaturi Fellowship in Biomedical Imaging Sciences at MIT.

[2] To whom correspondence should be addressed. E-mail: milanfar@unix.sri.com.

1. INTRODUCTION

In many applications of tomography, the aim is to extract a rather small set of geometrically based features from a given set of projection data [1–3]. In these instances, a full pixel-by-pixel reconstruction of the object is a rather inefficient and nonrobust approach. In addition, in many situations of practical interest, a full set of data with high signal-to-noise ratio (SNR) is often difficult, if not impossible, to obtain. Such situations arise in oceanography, nuclear medicine, surveillance, and nondestructive evaluation when due to the geometry of the object or the imaging apparatus, only a few noisy projections are available [4, 5]. In these cases, the classical reconstruction techniques such as filtered back-projection (FBP) [5] and algebraic reconstruction techniques (ART) fail to produce acceptable reconstructions. The shortcomings of these classical techniques in such situations can be attributed to two main sources. First, these techniques are invariably aimed at reconstructing every pixel value of the underlying object with little regard to the quality and quantity of the available data. To put it differently, there is no explicit or implicit mechanism to control greed and focus information, thus preventing one from attempting to extract more information from the data than it actually contains. The second type of shortcoming results from the fact that if we assume that the projection data are corrupted by Gaussian white noise, the process of reconstruction will have the net effect of "coloring" this noise. This effect manifests itself in the object domain in the form of spurious features which will complicate the detection of geometric features. This observation points out the importance of working directly with the projection data when the final goal is the extraction of geometric information. In our effort to address these two issues, we have proposed the use of simple *geometric* priors in the form of

1049-9652/94 $6.00
Copyright © 1994 by Academic Press, Inc.
All rights of reproduction in any form reserved.

finitely parameterized objects (namely, binary polygonal). The assumption that the object to be reconstructed is finitely parameterized allows for the tomographic reconstruction problem to be posed as a finite (relatively low-dimensional) parameter estimation problem. If we further assume, as we have done in the latter part of this paper, that the number of such parameters is also an unknown, we can formulate the reconstruction problem as a minimum description length estimation problem which provides for an automatic (data-driven) method for computing the optimal parameterized objects with the "best" number of parameters, given the data. This is, in essence, an information-theoretic criterion which gives us a direct way to estimate as many parameters as the information content of the data allows us to, and thus control the greed factor.

Other efforts in the parametric/geometric study of tomographic reconstruction have been carried out in the past. The work of Rossi and Willsky [6] and Prince and Willsky (see [7–9]) has served as the starting point for this research effort. In the work of Rossi, the object was represented by a known profile, with only four geometric parameters, namely, size, location, eccentricity, and orientation. These parameters were then estimated from projection data using the maximum likelihood (ML) formulation. In their approach, the number of unknown parameters was fixed and the main focus of their work was on performance analysis. Prince, on the other hand, used a priori information such as prior probabilities on sinograms and consistency conditions to compute maximum a posteriori (MAP) estimates of the sinogram and then used FBP to obtain a reconstruction. He made use of prior assumptions about shape, such as convexity, to reconstruct convex objects from support samples which were extracted from noisy projections through optimal filtering techniques. The approach of Prince provided an explicit method for integrating geometric information into the reconstruction process but was in essence still a pixel-by-pixel reconstruction. Extending these ideas, Lele and co-workers [10, 11] made use of only support information to produce polygonal reconstructions. Hanson [12] studied the reconstruction of axially symmetric objects from a single projection. Karl [13] also has studied the reconstruction of 3-D objects from 2-D silhouette projections.

The geometric modeling approach of Rossi and Willsky was expanded upon to include a more general set of objects by Bresler, Macovski, and Fessler (see [14–17]). In these papers, the authors chose sequences of 3-D cylinders and ellipsoids parameterized by stochastic dynamic models based on their radius, position, and orientation to model and reconstruct objects in two and three dimensions from projections.

Recently, Thirion [2] has introduced a technique to extract boundaries of objects from raw tomographic data through edge detection in the sinogram. Other work in geometric reconstruction by Chang [18] and more recently Kuba [19], Volcic [20], Fishburn *et al.* [21], and Gardner [22] has been concerned with the reconstruction of binary objects from only two noise-free projections.

Our approach provides a statistically *optimal* ML formulation for the direct recovery of vertices of binary polygons from the projection data in the presence of *noise*. We also provide an automatic mechanism for identifying the statistically optimal number of vertices, from a given data set. The statistically optimal ML formulation leads to an optimization problem that is *nonlinear* and filled with local extrema. An appropriate initial guess is thus essential for its iterative solution. An important contribution of this paper is that we thus provide a simple procedure to generate an appropriate initial guess based on moment estimates of the object computed from the original projection data.

The organization of this paper is as follows. In Section 2, we introduce the basic definitions and assumptions and pose the general problem which we intend to solve. We also discuss the particular statistical formulations of the reconstruction problem which we use. In particular, in Section 2.3, we discuss our novel technique for computing a good initial guess for the nonlinear optimization problems that result from our formulations. Section 3 contains basic performance results and robustness studies for various scenarios. Section 4 contains our conclusions.

2. THE RECONSTRUCTION PROBLEM

The Radon transform [5, 23] of a function $f(x, y)$ defined over a compact domain of the plane $\mathbb{O}$ is given by

$$g(t, \theta) = \int\int_{\mathbb{O}} f(x, y)\delta(t - \omega \cdot [x, y]^T)\, dx\, dy. \tag{1}$$

For every fixed t and θ, $g(t, \theta)$ is the line-integral of f over $\mathbb{O}$ in the direction $\omega = [\cos(\theta), \sin(\theta)]^T$, where $\delta(t - [\cos(\theta), \sin(\theta)] \cdot [x, y]^T)$ is a delta function on a line at angle $\theta + \pi/2$ and distance t from the origin. See Fig. 1.

Here we assume that the function f is the indicator function for some simply connected binary polygon and hence a finite set of parameters uniquely specify the function f. The estimation of the parameters that uniquely specify the function f is the concern of this paper. Let us stack the polygon vertices that uniquely define f in a vector V. We will assume throughout that the data available to us are discrete samples of g which are corrupted by Gaussian white noise of known intensity. In particular, our observations will be given by

$$Y_{i,j} = g(t_i, \theta_j, V^*) + w(t_i, \theta_j), \tag{2}$$

for $1 \le i \le m$, $1 \le j \le n$ where V^* is the true object we wish to reconstruct. The variables $w(t_i, \theta_j)$ are assumed

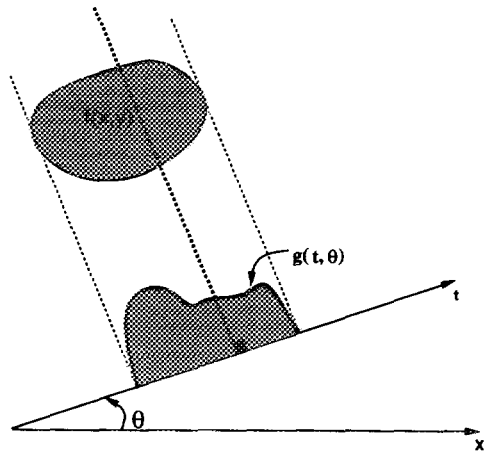

FIG. 1. The Radon transform.

to be independent, identically distributed (i.i.d.) Gaussian random variables with variance σ^2. We will denote by Y the vector of all such observations.

2.1. Maximum Likelihood Approach

In our approach, the original data in (2) are used to directly estimate the vertices V of a polygon in a statistically optimal way. The dimension of the parameter vector V (i.e., the number of sides) is determined by the level of detail that one can extract from the sparse and noisy data. For clarity, we first consider the case where a fixed and known number of vertices is assumed. In this case, the maximum likelihood [24] estimate, $\hat{V}_{\mathrm{ML}}$, of the parameter vector V is given by that value of V which makes the observed data most likely. In particular, using the monotonicity of the logarithm

$$\hat{V}_{\mathrm{ML}} = \arg\max_{V} \log[P(Y \mid V)], \tag{3}$$

where $P(Y \mid V)$ denotes the conditional probability density of the observed data set Y given the parameter vector V. It is well-known that given the assumption that the data is corrupted by i.i.d. Gaussian random noise, the solution to the above ML-estimation problem is precisely equivalent to the following nonlinear least-squares error (NLSE) formulation:

$$\hat{V}_{\mathrm{ML}} = \arg\min_{V} \sum_{i,j} \|Y_{i,j} - g(t_i, \theta_j, V)\|^2. \tag{4}$$

Formulation (4) shows that, in contrast to the linear formulation of classical reconstruction algorithms, the ML tomographic reconstruction approach, while yielding an optimal reconstruction framework, generally results in a highly nonlinear minimization problem. It is the nature of the dependence of g on the parameter vector V that makes the problem nonlinear.

Finally, note that if additional explicit geometric information is available in terms of a prior probabilistic description of the object vector V, then a maximum-a-posteriori estimate of V may be computed as follows:

$$\hat{V}_{\mathrm{MAP}} = \arg\max_{V} \log[P(V \mid Y)]. \tag{5}$$

In this work we concentrate on the ML problem given in (3) and its extensions, though application of our results to the MAP formulation is straightforward.

2.2. Minimum Description Length

In the previous ML discussion we assumed we had prior knowledge of the number of parameters describing the underlying object. Without this knowledge, we can consider the *minimum description length* (MDL) principal [25]. In this approach, the cost function is formulated such that the global minimum of the cost corresponds to a model of least order that explains the data best. The MDL approach in essence extends the maximum likelihood principal by including a term in the optimization criterion that measures the model complexity. In the present context, the model complexity refers to the number of vertices used to capture the object in question. Whereas the ML approach maximizes the log likelihood function given in (3), the MDL criterion maximizes a modified log likelihood function, as follows:

$$\hat{V}_{\mathrm{MDL}} = \arg\max_{V,N} \left\{ \log[P(Y \mid V)] - \frac{N}{2}\log(d) \right\}. \tag{6}$$

Here $d = mn$ is the number of samples of $g(t, \theta)$ and N refers to the number of parameters defining the reconstruction. Roughly speaking, the MDL cost is proportional to the number of bits required to model the observed data set with a model of order N, hence the term *minimum description length*. Under our assumed observation model (2) the MDL criterion (6) yields the following nonlinear optimization problem for the optimal parameter vector $\hat{V}_{\mathrm{MDL}}$:

$$\hat{V}_{\mathrm{MDL}} = \arg\min_{N} \min_{V} \left\{ \sigma^{-2} \sum_{i,j} \|Y_{i,j} - g(t_i, \theta_j, V)\|^2 + N\log(d) \right\}. \tag{7}$$

Here the optimization is now performed over both V and the number of parameters N. Note that the solution of the inner minimization in (7) essentially requires solution of the original ML problem (3) or (4) for a sequence of values of N.

Unless otherwise stated, we assume from here on that the *matrix* V contains the vertices of an N-sided binary,

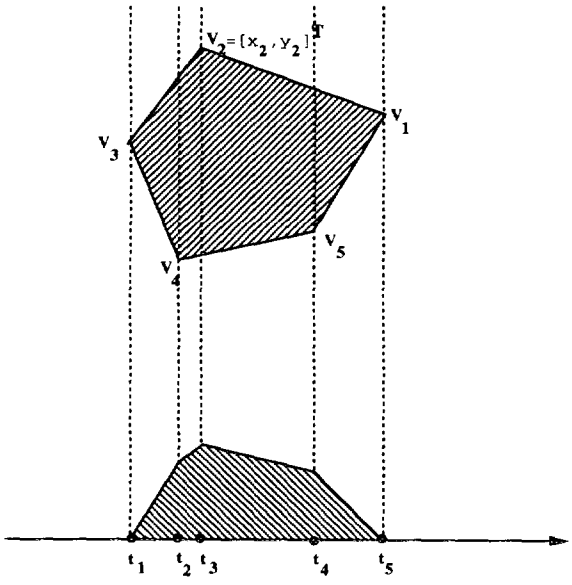

FIG. 2. A projection of a binary, polygonal object.

polygonal region as follows:

$$V = [V_1 | V_2 | \cdots | V_N]. \tag{8}$$

Here $V_i = [x_i, y_i]^T$ denotes the Cartesian coordinates of the ith vertex of the polygonal region arranged in the counterclockwise direction (see Fig. 2). Note that we use a matrix of parameters rather than a vector in what follows for notational convenience in the algorithms to follow, though this is not essential.

2.3. Algorithmic Aspects: Computing a Good Initial Guess

Given the highly nonlinear nature of the dependence of the cost function in (4) on the parameters in V, it appears evident that given a poor initial condition, typical numerical optimization algorithms may converge to local minima of the cost function. Indeed, this issue is a major obstacle to the use of a statistically optimal, though nonlinear, approach such as given in (3) or (6). In this section, we describe a method for using the projection data to directly compute an initial guess that is sufficiently close to the true global minimum as to, on average, result in convergence to it, or to a local minimum nearby. We do this by estimating the moments of the object directly from the projection data and then using (some of) these moments to compute an initial guess.

In considering the use of moments as the basis for an initialization algorithm, one is faced with two important issues. The first is that although estimating the moments of a function from its projections is a relatively easy task, as we have shown in [26, 27], the reconstruction of a function from a finite number of moments is in general a highly ill-posed problem even when these moments are exactly known [28]. Furthermore, in our framework the moments are estimated from noisy data, and hence are themselves noisy. In fact, as higher and higher order moments are estimated, the error in the estimates of these moments becomes larger. Our approach avoids these moment related difficulties by using the moments only to guide an initial coarse estimate of the object parameters for subsequent use in solution of the nonlinear ML or MDL problems. This initial estimate, in turn, itself mitigates the difficulties associated with the nonlinearities of the optimal statistical approaches. In particular, the amount of computation involved in arriving at an initial guess using our moment-based method is far smaller than the amount of computation (number of iterations) required to converge to an answer given a poor initial guess, especially since a poor initial guess may converge to a local minimum far from the basin of the global minimum. Further, the parameterization of the objects serves to regularize and robustify the moment inversion process [28–31].

Our method of using moments to generate an initial guess is based on the following set of observations. First, let μ_{pq}, $0 \le p, q$ denote the moment of $f(x, y)$ of order $p + q$ as given by

$$\mu_{pq} = \int\int x^p y^q f(x, y)\, dx\, dy. \tag{9}$$

In particular, note that the moments up to order 2 have the following physical relationships. The zeroth-order moment μ_{00} is the area of the object, the first-order moments μ_{01} and μ_{10} are the coordinates of the center of mass of the object scaled by the area, and the second-order moments μ_{02}, μ_{11}, μ_{20} are used to form the entries of the inertia matrix of the object. Thus these moments contain basic geometric information about object size, location, and elongation and orientation that, if available, could be used to guide our initialization of the nonlinear optimization problems (4) or (7). Our first aim then is to estimate them directly from the noisy projection data. To that end, it is easy to show that [23]

$$\int_{-\infty}^{\infty} g(t, \theta) t^k\, dt = \int\int_{\Re^2} f(x, y)[x \cos(\theta) + y \sin(\theta)]^k\, dx\, dy. \tag{10}$$

By expanding the integrand on the right hand side of (10), it becomes apparent that the moments of the projections are *linearly* related to the moments μ_{pq} of the object. In particular, specializing (10) to $k = 0, 1, 2$, and noting that $f(x, y)$ is an indicator function when the objects in question are binary, we arrive at the following relationships between μ_{pq}, $0 \le p + q \le 2$ and the projection $g(t, \theta)$ of $f(x, y)$ at each angle θ:

$$\mu_{00} = \int g(t, \theta)\, dt \equiv \mathcal{H}^{(0)}(\theta), \tag{11}$$

$$[\cos(\theta) \quad \sin(\theta)]\begin{bmatrix}\mu_{10}\\ \mu_{01}\end{bmatrix} = \int g(t,\theta)t\,dt \equiv \mathcal{H}^{(1)}(\theta), \quad (12)$$

$$[\cos^2(\theta) \quad 2\sin(\theta)\cos(\theta) \quad \sin^2(\theta)]\begin{bmatrix}\mu_{20}\\ \mu_{11}\\ \mu_{02}\end{bmatrix} = \int g(t,\theta)t^2\,dt \equiv \mathcal{H}^{(2)}(\theta). \quad (13)$$

Thus if we have projections at three or more distinct, known angles we can estimate the moments of up to order 2 of the object we wish to reconstruct. The computation of these moments is a *linear* calculation, making their estimation from projections straightforward (see [26]). Since, in general, many more than three projections are available, the estimation of these moments determining the area, center, and inertia axes of the object is overdetermined. The result is a robustness to noise and data sparsity through a reduction in the noise variance of their estimated values. In particular, we can stack the moments $\mathcal{H}^{(k)}(\theta_j)$ obtained from the projections at each angle θ_j to arrive at the following overall equations for the μ_{pq} up to order 2:

$$\begin{bmatrix}1\\ \vdots\\ 1\end{bmatrix}\mu_{00} = \begin{bmatrix}\mathcal{H}^{(0)}(\theta_1)\\ \vdots\\ \mathcal{H}^{(0)}(\theta_n)\end{bmatrix}, \quad (14)$$

$$\begin{bmatrix}\cos(\theta_1) & \sin(\theta_1)\\ \vdots & \vdots\\ \cos(\theta_n) & \sin(\theta_n)\end{bmatrix}\begin{bmatrix}\mu_{10}\\ \mu_{01}\end{bmatrix} = \begin{bmatrix}\mathcal{H}^{(1)(\theta_1)}\\ \vdots\\ \mathcal{H}^{(1)}(\theta_n)\end{bmatrix}, \quad (15)$$

$$\begin{bmatrix}\cos^2(\theta_1) & 2\sin(\theta_1)\cos(\theta_1) & \sin^2(\theta_1)\\ \vdots & \vdots & \vdots\\ \cos^2(\theta_n) & 2\sin(\theta_n)\cos(\theta_n) & \sin^2(\theta_n)\end{bmatrix}\begin{bmatrix}\mu_{20}\\ \mu_{11}\\ \mu_{02}\end{bmatrix} = \begin{bmatrix}\mathcal{H}^{(2)}(\theta_1)\\ \vdots\\ \mathcal{H}^{(2)}(\theta_n)\end{bmatrix}. \quad (16)$$

Using these equations we can easily calculate the least-squares (LS) estimates of the moments of the object μ_{pq} for $0 \le p + q \le 2$ given noisy observations of the moments of the projections. In particular, this is done by gathering the above sets of equations into a single linear equation of the form $\mathsf{h} = \mathsf{A}\mu + \mathsf{e}$, where h is the vector of *noisy* computed moments of the projections $\mathcal{H}^{(k)}(\theta_j)$ appearing above, and $\mu = [\mu_{00}, \mu_{10}, \mu_{01}, \mu_{20}, \mu_{11}, \mu_{02}]^T$, while e denotes a zero-mean vector of Gaussian noise with corresponding covariance matrix R which captures the noise in our observations of $\mathcal{H}^{(k)}(\theta_j)$. This noise model, of course, follows directly from that of (2). The least-squares estimate of the vector μ is then given by

$$\hat{\mu} = (\mathsf{A}^T\mathsf{R}^{-1}\mathsf{A})^{-1}\mathsf{A}^T\mathsf{R}^{-1}\mathsf{h}. \quad (17)$$

Note that if this least-squares estimate is consistent,[3] it will coincide with the optimum maximum likelihood estimate of the moments of the underlying polygon. The estimates of the low-order moments, such as those we use here, are robust to noise in the data and hence in the great majority of the cases, the LS estimate does indeed coincide with the ML estimate. When this fails, it is typically due to the inconsistency of the second-order moment estimates. In such cases, we refrain from using the second-order estimates and build our initial guess using only the area and center of mass estimates as we describe next. (The general framework for the optimal estimation of the moments of any order of a function $f(x, y)$ from noisy measurements of its Radon transform is developed in [26, 27].) We shall henceforth denote the LS moment estimates by $\hat{\mu}_{pq}$.

Now that we have estimates of the moments of up to order 2 of the object, and thus estimates of its basic geometric structure, we need to convert this information into a suitable object for use in initializing the nonlinear optimization problem (4) or (7). The initial guess algorithm outlined next uses these least squares estimates of the low-order moments $\hat{\mu}_{pq}$, obtained from the noisy projection data, to produce a polygon which has moments up to order 2 which are close to (or in some cases equal to) those which were estimated from the projection data. The resulting polygon, which will be used as our initialization, should thus have the same basic geometric structure as the underlying object.

Recall that in this process of generating an initial object from the moment data we want to avoid the difficulties usually associated with obtaining an object from a set of its moments [28–31]. For this reason, the initial polygon we will use is simply obtained as the affine transformation of a reference object $V_{\text{ref}}(N)$, which is a centered regular N-gon of unit area. For a given choice of number of sides N, the reference object we use is given by

$$V_{\text{ref}}(N) = \frac{1}{\sqrt{(N/2)\sin(2\pi/N)}}\begin{bmatrix}\cos(0) & \cos\left(\frac{2\pi}{N}\right) & \cdots & \cos\left(\frac{2\pi(N-1)}{N}\right)\\ \sin(0) & \sin\left(\frac{2\pi}{N}\right) & \cdots & \sin\left(\frac{2\pi(N-1)}{N}\right)\end{bmatrix}. \quad (18)$$

[3] That is, it satisfies the necessary and sufficient conditions to be the moment vector of some binary polygon, e.g., give a positive area estimate and a positive definite inertia matrix estimate. We have dealt with the inconsistent moment case directly in [26].

The affine transformation of this reference object, which will be generated from the estimated moment set, consists of a uniform scaling, a stretching along the coordinate axes, a rotation, and finally a translation, and simply corresponds to the following transformation of the underlying spatial coordinates of the reference object

$$\begin{bmatrix} x' \\ y' \end{bmatrix} = L \begin{bmatrix} x \\ y \end{bmatrix} + C. \tag{19}$$

In particular, given the form of $V_{\text{ref}}(N)$ in (18), this yields the following equation for the family of possible initial objects V_{init}:

$$V_{\text{init}} = LV_{\text{ref}}(N) + [C \mid \cdots \mid C]. \tag{20}$$

The set of all such affine transformations of $V_{\text{ref}}(N)$ we term the *affinely regular* N-gons [32]. In the absence of noise, the initial guess algorithm we detail will exactly match the given estimated moments if the underlying object itself happens to be affinely regular. If the underlying object is not affinely regular itself, the algorithm will not necessarily produce an N-gon exactly matching its moments, even in the absence of noise, though as we will show, it will usually be close. Of course, in the presence of noise the estimated moments themselves are not exact and thus, while we would hope to get close, our resulting initial N-gon will never exactly match the true moments of the underlying object anyway.

Given that we will restrict ourselves to initial objects of the form (20), let us consider how we might choose the parameters of the transformation L and C to match a given estimated moment set $\hat{\mu}_{pq}$, $0 \le p + q \le 2$. Using (20) and (18) to calculate the moments of V_{init} up to order 2, we obtain the relationships

$$\mu_{00}(V_{\text{init}}) = |\det(L)|, \tag{21}$$

$$\begin{bmatrix} \mu_{10}(V_{\text{init}}) \\ \mu_{01}(V_{\text{init}}) \end{bmatrix} = |\det(L)|C, \tag{22}$$

$$\begin{bmatrix} \mu_{20}(V_{\text{init}}) & \mu_{11}(V_{\text{init}}) \\ \mu_{11}(V_{\text{init}}) & \mu_{02}(V_{\text{init}}) \end{bmatrix} = |\det(L)|(k_N LL^{\mathrm{T}} + CC^{\mathrm{T}}), \tag{23}$$

where $\mu_{pq}(V_{\text{init}})$ is the pqth moment of V_{init} and $k_N = 1/(4N \tan(\pi/N))$. Thus to match $\mu_{00}(V_{\text{init}})$, $\mu_{10}(V_{\text{init}})$, $\mu_{01}(V_{\text{init}})$ with their estimated counterparts, the first two conditions require that

$$|\det(L)| = \hat{\mu}_{00} \tag{24}$$

$$C = \frac{1}{\hat{\mu}_{00}} \begin{bmatrix} \hat{\mu}_{10} \\ \hat{\mu}_{01} \end{bmatrix}. \tag{25}$$

The first condition simply corresponds to a scaling of $V_{\text{ref}}(N)$ so that its area matches the estimated one. The second condition shows that the affine term C in the transformation (19) should correspond to a translation of $V_{\text{ref}}(N)$ to the estimated center of mass of the object. These two conditions assure that we match the estimated area and center of mass location.

Now, after some manipulation, (23) implies that to match the estimated second-order moments $\hat{\mu}_{pq}$, $p + q = 2$, we must have

$$LL^{\mathrm{T}} = \frac{1}{k_N \hat{\mu}_{00}} \hat{\mathcal{J}}, \tag{26}$$

where $\hat{\mathcal{J}}$ is the matrix of estimated central moments defined by

$$\hat{\mathcal{J}} = \begin{bmatrix} \hat{\mu}_{20} & \hat{\mu}_{11} \\ \hat{\mu}_{11} & \hat{\mu}_{02} \end{bmatrix} - \frac{1}{\hat{\mu}_{00}} \begin{bmatrix} \hat{\mu}_{10} \\ \hat{\mu}_{01} \end{bmatrix} [\hat{\mu}_{10} \quad \hat{\mu}_{01}]. \tag{27}$$

In particular, this condition implies another constraint on $\det(L)$ independent of (24), which we will not, in general, be able to satisfy. Specifically, a necessary condition for finding an L satisfying both (26) and (24) is that

$$\det(\hat{\mathcal{J}}) = k_N^2 \hat{\mu}_{00}^4. \tag{28}$$

Actually, as shown in Appendix A, condition (28) is also sufficient. Clearly, this condition will not, in general, be satisfied and we will be unable to exactly match the estimated second moments. In fact, the objects that do meet this constraint, and thus whose moments we can exactly match, are precisely the elements of the set of affinely regular N-gons. Geometrically, this situation reflects the limitation of our restricted initial guess object class (20), i.e., the set of affinely regular N-gons. Within this class, for a given object area we are constrained as to the "size" of the corresponding inertia matrix we may have, where inertia size is measured as the product of the principal central inertia moments (eigenvalues of the central inertia matrix). For example, while our initial guess objects will always be convex polygons, for a given area we can always obtain nonconvex objects of greater inertia by "moving area outward," as in a dumbell.

The condition (26) can also be viewed as implying a different scaling on L needed to obtain a perfect match to the inertia condition. In general, we thus have a choice of picking this scaling of L to satisfy either the inertia condition (26) or the area condition (24). Since the area condition (24) is both a more robustly estimated and a more fundamental geometric quantity, we choose to enforce this condition in the algorithm to follow. We then choose L so that the resulting central inertia matrix of V_{init} has the same principal axes directions and has its

principal inertias in the same ratio as those estimated from the data as found in $\hat{\mathcal{I}}$. We accomplish these goals by using a square root of the matrix $\hat{\mathcal{I}}$ normalized to have unit determinant for the form of L, then scaling the result to match the determinant condition (24). Thus we sacrifice overall scaling of the inertia matrix in favor of matching the estimated area. Collecting the above steps and reasoning, the overall algorithm is given by the following:

ALGORITHM 1 (Initial Guess Algorithm). 1. Compute the least-squares estimates of the moments up to order 2 ($\hat{\mu}_{00}$, $\hat{\mu}_{10}$, $\hat{\mu}_{01}$, $\hat{\mu}_{20}$, $\hat{\mu}_{11}$, and $\hat{\mu}_{02}$) from the raw projection data using (14)–(17).

2. Construct an N-sided regular polygon centered at the origin with vertices chosen as the scaled roots of unity in counterclockwise order so that they lie on the circle of radius $1/\sqrt{(N/2)\sin(2\pi/N)}$. This polygon has unit area and is defined in Eq. (18).

3. Compute the translation C, obtained as the estimated object center of mass:

$$C = \frac{1}{\hat{\mu}_{00}} \begin{bmatrix} \hat{\mu}_{10} \\ \hat{\mu}_{01} \end{bmatrix}. \tag{29}$$

4. Form the estimated central inertia matrix $\hat{\mathcal{I}}$ from the estimated moments according to (27).

5. If $\hat{\mathcal{I}}$ is not positive definite, set $L = \sqrt{\hat{\mu}_{00}} I_2$ and goto step 8. Otherwise proceed to step 6. (I_2 is the 2×2 identity matrix.)

6. Perform an eigendecomposition of the normalized matrix $\hat{\mathcal{I}}$ as follows:

$$\frac{\hat{\mathcal{I}}}{\sqrt{\det(\hat{\mathcal{I}})}} = U \begin{bmatrix} \lambda & 0 \\ 0 & 1/\lambda \end{bmatrix} U^{\mathrm{T}}. \tag{30}$$

Here we have assumed that the eigenvalues are arranged in descending order and that the eigenvectors are normalized to unit length so that $\det(U) = \pm 1$. Note that the eigenvalues are reciprocals of each other since we have scaled the left hand side so that its determinant is 1.

7. Form the linear transformation L as a scaled square root of $\hat{\mathcal{I}}$ as follows:

$$L = \sqrt{\hat{\mu}_{00}}\, U \begin{bmatrix} \sqrt{\lambda} & 0 \\ 0 & 1/\sqrt{\lambda} \end{bmatrix}. \tag{31}$$

Note that $\det(L) = \hat{\mu}_{00}$ as desired. Depending on whether U is a pure rotation or a rotation followed by a reflection, it will have determinant $+1$ or -1, respectively. Also note that we use this (Schur decomposition-based) square root formulation over the more numerically attractive Cholesky factorization since our choice leads to matrices that are directly interpretable as rotations, reflections, and scalings.

8. The initial guess V_{init} is now obtained by applying the scaling, stretching, and rotation transformation L and the translation C to the reference object $V_{\text{ref}}(N)$ via the coordinate transformation $[x', y']^{\mathrm{T}} = L[x, y]^{\mathrm{T}} + C$. Because of the form of $V_{\text{ref}}(N)$ this operation yields

$$V_{\text{init}} = LV_{\text{ref}}(N) + [C \,|\, \cdots \,|\, C]. \tag{32}$$

Note that the eigenvalue λ of the unit determinant matrix calculated in step 7 gives the eccentricity of the underlying object while the corresponding eigenvectors give its orientation. Also note that in the presence of noise the estimated central inertia matrix for the object $\hat{\mathcal{I}}$ may not be strictly positive definite and hence may not correspond to the inertia matrix of any object at all. In such instances, the algorithm refrains from the use of these moments of order 2 and computes an initial guess based only on the estimated area and center of mass.

If the matrix L, computed above, is replaced by $L' = LT$ for any orthogonal T, the resulting quantity $L'L'^{\mathrm{T}}$ satisfies

$$LL^{\mathrm{T}} = L'L'^{\mathrm{T}}. \tag{33}$$

Hence, although the initial guess generated by the above algorithm is unambiguous and unique in the sense that the square root of $\hat{\mathcal{I}}$ obtained by the algorithm is unique, an infinity of other initial guesses having the same moments up to order 2 may be generated by replacing L by LT and allowing T to range over the set of all 2×2 orthogonal transformations. A precise characterization of this set of all affinely regular N-gons with the same moments up to order 2 is, in fact, given in the following result, which we prove in Appendix A.

RESULT 1. *Consider the set of all N-gons with moments up to order 2: μ_{00}, μ_{10}, μ_{01}, μ_{20}, μ_{11}, μ_{02}, such that the resulting inertia matrix*

$$\mathcal{I} = \begin{bmatrix} \mu_{20} & \mu_{11} \\ \mu_{11} & \mu_{02} \end{bmatrix} \tag{34}$$

satisfies $\det(\mathcal{I}) = k_N^2 \mu_{00}^4$. *This set coincides with the set of N-gons with vertices on an ellipse $\mathcal{E}_O$ and sides tangent, at their midpoints, to a confocal ellipse $\mathcal{E}_I$, where these ellipses are given by*

$$\mathcal{E}_O = \{\mathbf{z} \,|\, (\mathbf{z} - C)^{\mathrm{T}} E_O^{-1} (\mathbf{z} - C) = 1\} \tag{35}$$

$$\mathcal{E}_I = \{\mathbf{z} \,|\, (\mathbf{z} - C)^{\mathrm{T}} E_I^{-1} (\mathbf{z} - C) = 1\}. \tag{36}$$

with

$$C = \frac{1}{\mu_{00}} \begin{bmatrix} \mu_{10} \\ \mu_{01} \end{bmatrix} \tag{37}$$

$$E_O = \frac{4}{\mu_{00}\cos^2(\pi/N)}\mathcal{J} \tag{38}$$

$$E_I = \frac{4}{\mu_{00}}\mathcal{J}. \tag{39}$$

This result states that the class of all affinely regular N-gons with a given set of moments up to order 2 is given by the class of N-gons whose vertices are on a fixed ellipse and whose side are tangent to a second ellipse which is confocal with the first. (See Fig. 3 for an example.) The ellipses are uniquely determined by the values of the given moments. The above result draws attention to a question of a more general nature; namely, "How many moments (and hence projections) uniquely specify a simply-connected N-gon?". We answer this question in [33] and [26] where in the former we have shown that moments up through order $2N - 3$ suffice to uniquely specify the vertices of any simply connected N-gon, while in the latter we have shown that $m + 1$ projections are necessary and sufficient to uniquely specify the moments up through order m of *any object* from its projections. Hence, together these results show that with $2N - 2$ projections, we can uniquely specify the vertices of any N-sided, simply connected polygon. In contrast to [33, 26] where image reconstruction from projections is based directly on the estimated moments, the Initial Guess Algorithm presented here aims only to give a rough initial guess which is hopefully within a reasonable neighborhood of the global optimum of the ML cost.

In order to simplify the Initial Guess algorithm, we do not search further over the family given by Result 1. We simply use the output of the Initial Guess Algorithm described above as the starting guess for our nonlinear optimization routines.

3. EXPERIMENTAL RESULTS

In this section, we present some performance studies of our proposed algorithm with simple polygonal objects as prototypical reconstructions. One may expect that our algorithms work best when the underlying object (that from which the data is generated) is itself a simple binary polygonal shape. While this is true, we will also show that our algorithms perform well even when the underlying objects are complex, nonconvex, and nonpolygonal shapes.

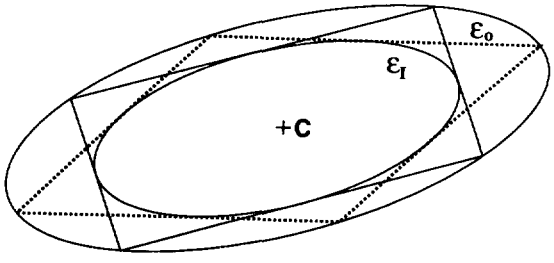

FIG. 3. Illustration of Result 1.

First we demonstrate reconstructions based on the ML criterion. In these reconstructions we use the parameters of the true polygon as the initial guess. Typical reconstructions are shown along with average performance studies for a variety of noise and data sampling scenarios. In particular, we show that given a good initial guess, the performance of our algorithms is quite robust to noise and sparsity of the data, significantly more so than classical reconstruction techniques. To demonstrate this point, reconstructions using our techniques and the classical FBP are provided.

Next we demonstrate how the MDL criterion may be used to optimally estimate the number of parameters (sides) N directly from the data. We solve these MDL problems by solving the ML problem for a sequence of values of N. To initialize each of these ML problems, the Initial Guess Algorithm was used. The robustness of the MDL approach and its ability to capture the shape information in noisy data when the underlying object is not polygonal is also shown through polygonal reconstruction of more complicated shapes. Two remarks are in order regarding the results presented in Section 3.1. The first is that the results in this section, begin by initializing the algorithms with the true underlying polygon. This corresponds to local exploration of the ML and MDL cost functions. Hence, any interpretation of these performance results (e.g., robustness) is conditioned on whether or not the Initial Guess Algorithm will provide a starting guess that is within the local basin of the global optimum (which as we show in Section 3.1 apparently includes the underlying polygon). In the subsequent sections, we show that the Initial Guess Algorithm does, on average, place the starting values in a reasonable neighborhood of the global optimum.

The second remark is that the ML, and indeed the MDL, formulations are not based upon whether the underlying polygon is affinely regular, or even convex. Hence, although our algorithms may, in general, yield nonaffinely regular or even nonconvex solutions, they generally perform best when the underlying polygon is itself affinely regular; this is a direct consequence of the fact that the Initial Guess Algorithm always yields an affinely regular polygon. In Section 3.4, we report studies in which the Initial Guess Algorithm is used to produce a starting guess for the optimization routines. In these studies, we show that although the performance of the overall algorithm does degrade somewhat, this degradation in performance is not significant.

In order to quantify some measure of performance of our proposed reconstruction algorithms, we first need to

define an appropriate notion of signal-to-noise ratio (SNR). We define the *SNR per sample* as

$$\text{SNR} = 10 \log_{10} \frac{\sum_{i,j} g^2(t_i, \theta_j)/d}{\sigma^2}, \tag{40}$$

where $d = m \times n$ is the total number of observations, and σ^2 is the variance of the i.i.d. noise w in the projection observations (2).

In all our simulations, the reconstruction error is measured in terms of the percent Hausdorff distance [32] between the estimate and the true polygon or shape. The Hausdorff metric is a proper notion of "distance" between two nonempty compact sets and it is defined as follows. Let $d(p^*, S)$ denote the minimum distance between the point p^* and the compact set S:

$$d(p^*, S) = \inf\{\|p^* - p\| \mid p \in S\}. \tag{41}$$

Define the *ε-neighborhood* of the set S as

$$S^{(\varepsilon)} = \{p \mid d(p, S) \leq \varepsilon\}. \tag{42}$$

Now given two nonempty compact sets, S_1 and S_2, the Hausdorff distance between them is defined as

$$\mathcal{H}(S_1, S_2) = \inf\{\varepsilon \mid S_1 \subset S_2^{(\varepsilon)} \text{ and } S_2 \subset S_1^{(\varepsilon)}\} \tag{43}$$

In essence, the Hausdorff metric is a measure of the largest distance by which the sets S_1 and S_2 differ. The *percent* Hausdorff distance between the true object S and the reconstruction $\hat{S}$ is now defined as

$$\text{Percent Error} = 100\% \times \frac{\mathcal{H}(\hat{S}, S)}{\mathcal{H}(O, S)}, \tag{44}$$

where O denotes the set composed of the single point at the origin, so that if S contains the origin, $\mathcal{H}(O, S)$ is the maximal distance of a point in the set to the origin and thus a measure of the set's size.

In all experiments that follow, the field of view (the extent of measurement in the variable t) is taken to be twice the maximum width of the true object. While it is true that significantly enlarging the field of view will certainly degrade the performance of the proposed algorithms, our choice to fix this at twice the size of the true object is not unjustified or arbitrary. In fact, we are assuming that a mechanism exists, such as that reported in [7], whereby a rough estimate of the maximal support of the object may be estimated from the raw projection data in a statistically optimal fashion.

The numerical algorithm used to solve the optimization problems presented in this paper was the Nelder–Mead simplex algorithm [34]. The specific stopping criterion was to declare a solution after the cost failed to decrease by more than 10^{-4} in 50 iterations, or after 500 iterations of the Nelder–Mead algorithm; whichever came first.

Finally, as for the assumption that the underlying object is simply connected, we did not explicitly enforce this on the solution. Having obtained a solution (vertices) from the numerical search algorithm, we essentially connected the vertices in such a way as to minimize the cost.

3.1. ML-Based Reconstruction

Here we present examples and performance analyses of the ML-based reconstruction method (4). As we alluded to before, the studies reported here correspond to a local exploration of the ML cost function. To this end, we set the initial guess equal to the true object. While there is no guarantee that this choice of initial guess will result in convergence to the global optimum (especially given the presence of noise in the data), the resulting reconstructions suggest that this initialization typically yields solutions that are at least very near the global optimum.

3.1.1. *Sample Reconstructions*

In Figs. 4 and 5, we show optimal reconstructions of a triangle and a hexagon, respectively, based on the ML criterion. The true polygon, in each case is depicted in solid lines, while the estimate is shown in dashed lines. For both objects, 1000 noisy projection samples were collected in the form of 50 equally spaced projections in the interval $(0, \pi]$ ($m = 50$), and 20 samples per projection ($n = 20$). The field of view (extent of measurements in

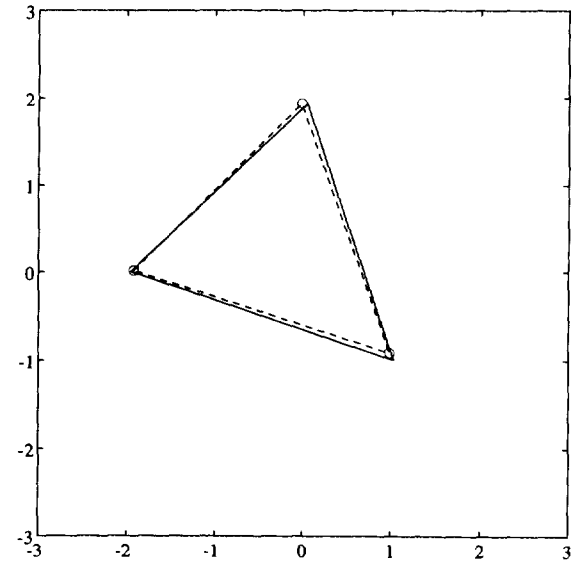

FIG. 4. Triangle example: SNR = 0 dB, 50 views, 20 samples/view; true (—) and reconstruction (- -); % error = 7.2.

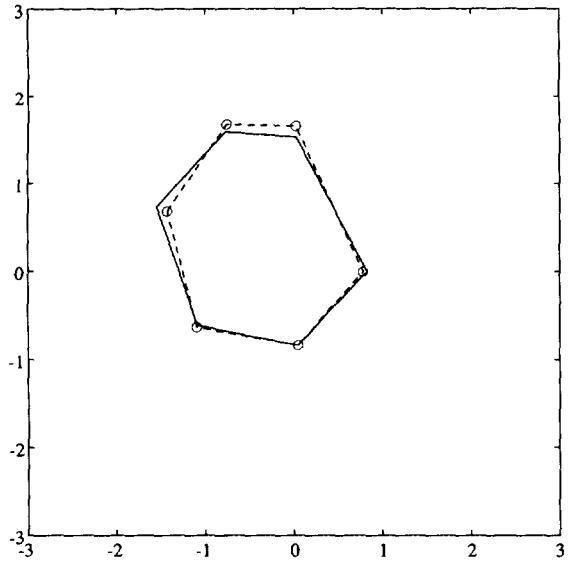

FIG. 5. Hexagon example: SNR = 0 dB, 50 views, 20 samples/view; true (—) and reconstruction (- -); % error = 9.6.

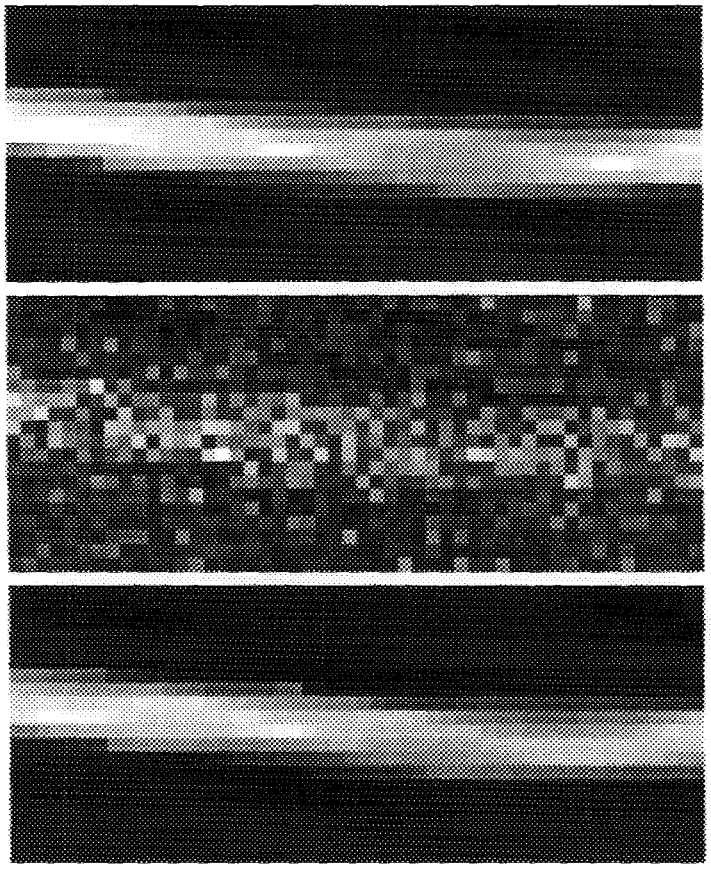

FIG. 6. From top to bottom: Sinograms with 50 projections and 20 samples per projection of (I) noiseless hexagon, (II) noisy data at 0 dB, and (III) reconstructed hexagon. In each of these images, the horizontal axis is θ, the vertical axis is t, and the intensity values are the values of the corresponding projections mapped to the grayscale range [0, 255].

the variable t) was chosen as twice the maximum width of the true object in each case. For each of these data sets the variance of the noise in (2) was set so that the SNR given by (40) was equal to 0. The typical behavior of the optimal ML-based reconstructions in the projection space can be seen in Fig. 6, which corresponds to the hexagon of Fig. 5. The top image of this figure shows the underlying projection function $g(t_i, \theta_j, V^*)$ of (2) for the hexagon, while the middle image shows the noisy observed data $Y_{i,j}$. The object is difficult to distinguish due to the noise in the image. The bottom image shows the reconstructed projections corresponding to the optimal estimate $g(t_i, \theta_j, \hat{V})$, which are virtually indistinguishable from those corresponding to the true object. Figure 7 shows the best FBP reconstruction of the hexagon used in Fig. 5 based on 4096 projection samples of the same SNR (0) (64 angles with 64 samples per angle). For comparison, the reconstruction from this data using our algorithm is shown in Fig. 8. (Note here that what constitutes the "best" FBP is somewhat subjective. We tried many different filters and visually, the best reconstruction was obtained with a Butterworth filter of order 3 with 0.15 normalized cutoff frequency.)

Note that the number of samples per projection used in this reconstruction is actually *more* than the number used to produce the ML-based reconstruction in Fig. 5. The increase in sampling was necessary because FBP produces severe artifacts if the number of views exceeds the number of samples per view [5]. The ML approach

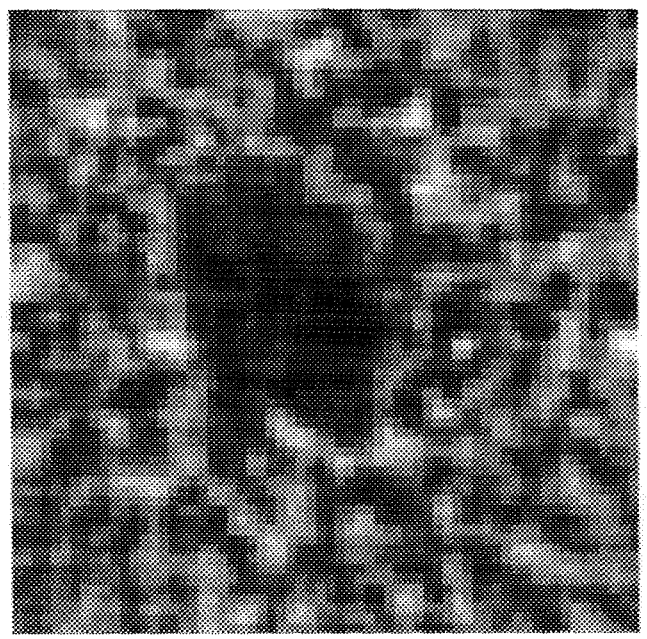

FIG. 7. Sample reconstruction of a hexagon at 0 dB SNR using FBP: 64 views, 64 samples per view.

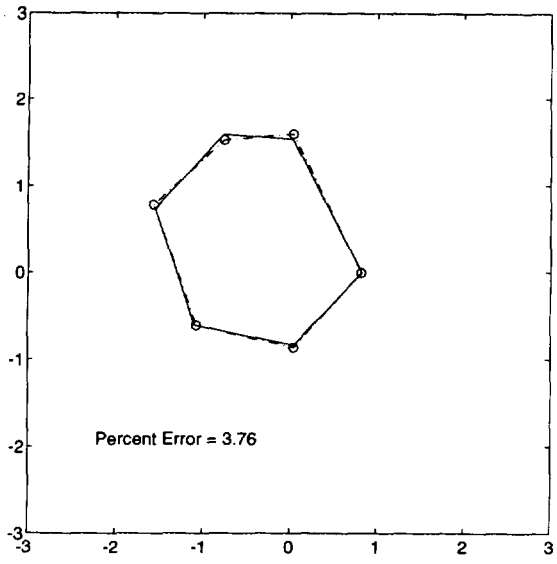

FIG. 8. Sample reconstruction of a Hexagon at 0 dB SNR, 64 views, 64 samples/view; true (—) and reconstruction (- -).

has no such difficulties, as we will see in the next section, where we examine performance.

In contrast to the ML-based reconstruction, the details of the hexagon are corrupted in the FBP reconstruction. In addition, there are spurious features in the FBP reconstructions and perhaps most importantly, to extract a binary object from the FBP reconstruction, we would need to threshold the image or perform edge detection on it. Neither of these postprocessing steps are easily interpretable in an optimal estimation framework and, of course, they incur even more computational costs.

3.1.2. *Effect of Noise on Performance*

The average performance of the ML-based reconstructions is presented through several Monte Carlo studies. Again, for these experiments an initial condition equal to the true object was used in each case to ensure that we obtain the actual ML estimates. The first study establishes average reconstruction errors at various SNRs for a fixed number of data samples. The purpose of these simulations is to demonstrate that the ML-based reconstructions are robust to the quality of the data used for a wide range of SNRs. The same two polygons as in Figs. 4 and 5 were chosen as the underlying objects. Again, in each case, 1000 samples of the projections of these objects were collected in the form of 50 equally spaced projections in the interval $(0, \pi]$ ($m = 50$), and 20 samples per projection ($n = 20$), while the field of view (extent of measurements in the variable t) was chosen as twice the maximum width of the object in each case. The samples $g(t_i, \theta_j, V^*)$ were then corrupted by Gaussian white noise $w(t_i, \theta_j)$ of different intensities to yield data sets at several SNRs. At each SNR, 100 reconstructions were done using independent sample paths of the corrupting white noise. The average reconstruction error was then computed and is displayed versus the SNR in Fig. 9. The error bars denote the 95% confidence intervals for the computed mean values.

The percent error in these reconstructions increases with decreasing SNR, as one would expect. In fact, the graph shows that, at least in the examined SNR range of -4.35 to $+4.35$ dB, the relation between percent error and SNR is roughly linear in the cases of the triangle and the hexagon. This suggests that given a good initial guess, the performance of our algorithm does not degrade very fast with decaying SNR, demonstrating the robustness to noise of such object-based optimal ML estimates.

3.1.3. *Effect of Sampling on Performance*

Here the performance of our ML-based estimates with respect to both the number of available data samples and their distribution is studied. One would naturally expect that as the number of available data points decreases, the reconstruction error should increase. The main aim of these simulations is to demonstrate that given a good initial guess, the ML-based reconstructions are robust to both the quantity and the distribution of data over a wide range of SNRs. In particular, reasonable estimates are produced even with a drastic reduction of data and, unlike the behavior seen in FBP reconstructions, the ML estimates display no catastrophic degradation as the samples per angular view are reduced. The *relative* sensitivity of the ML estimates to density of samples of $g(t, \theta, V^*)$ in t and θ is also discussed, providing information of use for the design of sampling strategies.

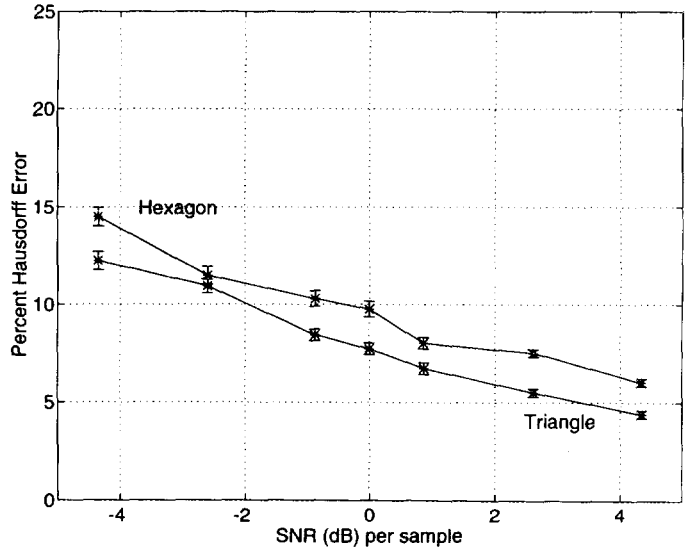

FIG. 9. Mean performance curves for ML reconstructions of a triangle and a hexagon.

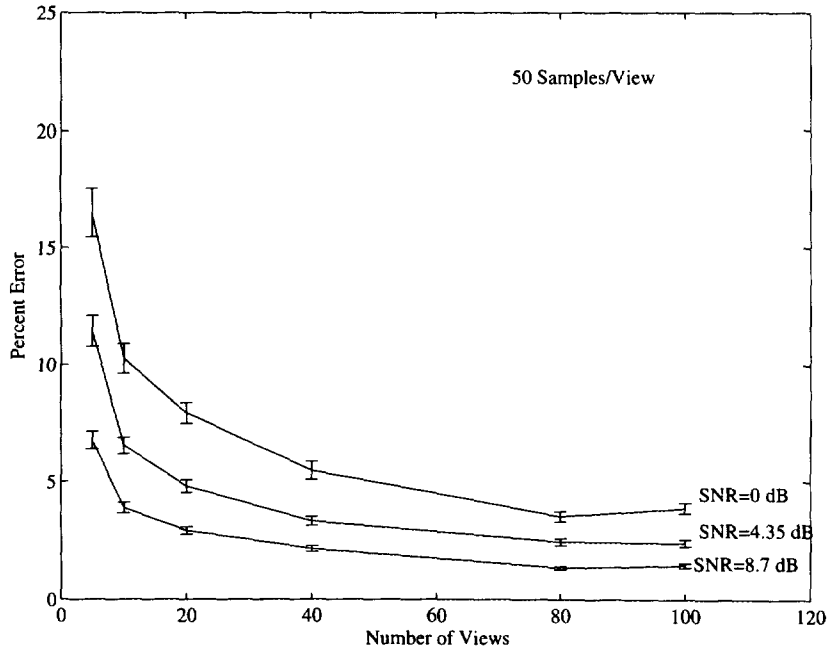

FIG. 10. Performance as a function of number of views.

The true hexagon used in Fig. 5 was again used as the underlying object. As before, an initial condition equal to the true object was used for each of experiments. A series of Monte Carlo simulations (50 runs for each sampling configuration) were then performed at various SNRs to observe the effect of sparse projections and sparse sampling in each projection. In Fig. 10, the percent Hausdorff reconstruction error is plotted versus the number of angular views for SNRs of 0, 4.35, and 8.7 dB, while the number of samples per view was fixed at 50. With a modest 50 samples per view, all three curves fall below 10% reconstruction error when the number of views is greater than about 10. This is only 500 total observations, many of which do not contain the object at all (since the field of view is twice as large as the object). Furthermore, as the number of angular views is decreased from 100 to 10, only a marginal increase in the reconstruction error is observed. These observations testify to the robustness of the ML algorithm with respect to the number of views when a good initial guess is given.

In Fig. 11, the dual case is presented. In this figure, the percent Hausdorff reconstruction error is plotted versus the number of samples per view for SNRs of 0, 4.35, and 8.7 dB, while the number of angular views was fixed at 50. With 50 angular views, all curves fall below 10% reconstruction error when the number of samples per view is greater than only 10. Also, as the number of samples per view is decreased from 100 to 10, again only a marginal increase in the reconstruction error is observed. This behavior shows that the ML algorithm is robust with respect to the number of samples per view when a good initial guess is given. Note that for a fixed sampling strategy, the reconstruction error increases only slightly as the SNR is decreased over a wide range. For instance, in Fig. 10, with 40 angular views and 50 samples per view, the percent error is reduced only about 5% while the SNR goes from 0 to 8.7 dB.

Finally, it is noteworthy that the reconstruction error enjoys a dramatic improvement for all SNRs (0, 4.35, and 8.7 dB) when the number of samples per view is increased from 5 to 10. This improvement is more significant than that observed in Fig. 10 when the number of views is increased from 5 to 10. This behavior indicates that in a scenario where only a small (fixed) number of sample points can be collected, it is more beneficial to have more samples per view rather than more views.

3.2. MDL Reconstructions

Here we will examine reconstruction under the MDL criterion of (7) where we now assume that the number of sides of the reconstructed polygon is unknown. In particular, the reconstruction experiments for the hexagon in Fig. 5 were repeated in SNR = 0 dB assuming no knowledge of the number of sides. The MDL criterion was employed to estimate the optimal number of sides. As in the ML algorithm, it is important to find a good initial guess for the MDL algorithm as well. The problem is twofold. First, a reasonable guess must be made as to the appropriate *range* of the number of sides. We picked a fairly small

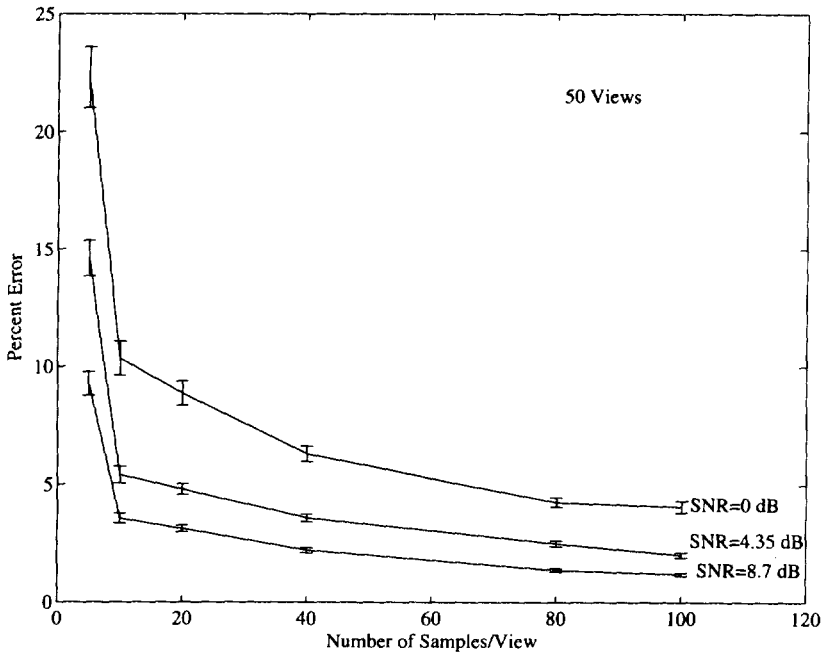

FIG. 11. Performance as a function of number of samples per view.

range for the number of sides of the reconstruction, typically, 3 to 10 sides. Next, for each number of sides, the Initial Guess Algorithm was used to produce an initial guess to the optimization routine. The method for selecting the range of the number of sides is ad hoc, but was shown to be reliable in the sense that for our simulations, the MDL cost never showed local or global minima for convex objects with number of sides larger than 10. Figure 12 shows a plot of the MDL cost corresponding to the expression in (7) versus the number of sides for a sample reconstruction of the hexagon in Fig. 5. It can be seen that the minimum occurs at $N = 6$, demonstrating that the optimal MDL reconstruction will consist of 6 sides. Indeed this number coincides with the true number of

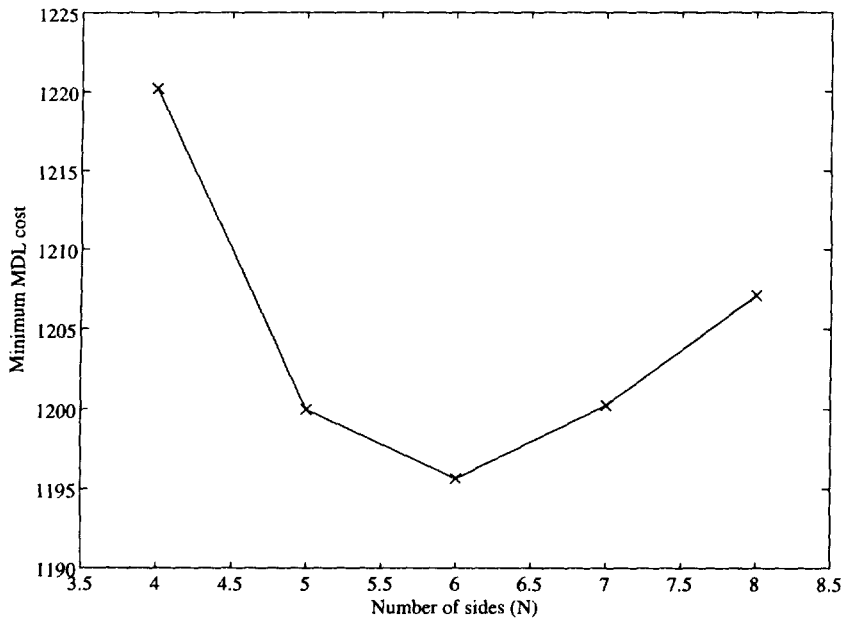

FIG. 12. Cost vs number of sides for the hexagon in Fig. 5.

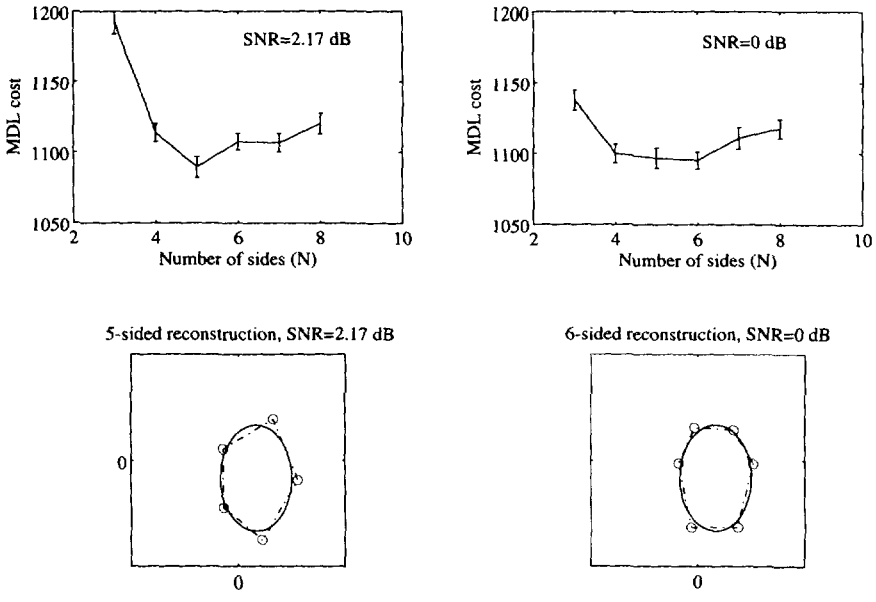

FIG. 13. Minimum MDL costs and sample reconstruction for an ellipse.

sides of the underlying object. The optimal MDL estimate is thus exactly the optimal ML estimate for this data set presented before.

3.3. Polygonal Reconstruction of Nonpolygonal Objects

In this section, we wish to study the robustness of MDL-based estimates when the underlying, true object is nonpolygonal. First, we examine the case of an elliptical object. We use the MDL formulation presented in the previous section and study the behavior of the optimal reconstructions at two different SNRs. To this end, let the true object (that which generated the data) be a binary ellipse whose boundary is given by

$$\left\{x, y \,\middle|\, \left(x - \frac{1}{2}\right)^2 + \frac{(y + 1/2)^2}{9/4} = 1\right\}. \tag{45}$$

The above relation defines an ellipse centered at the point $(1/2, -1/2)$ whose major and minor axes are aligned with the coordinate axes with lengths 1 and 3/2, respectively.

One thousand (1000) noisy samples of the Radon transform of this ellipse were generated ($m = 50$ equally spaced angular views in $(0, \pi]$, and $n = 20$ samples per view) at SNRs of 0 and 2.17 dB, respectively, for 50 different sample paths of the corrupting noise. For each set of data, reconstructions were performed using the ML algorithm with 3, 4, 5, 6, 7, and 8 sides together with the Initial Guess Algorithm. The MDL cost in (7) was then computed for each of these reconstructions. The ensemble mean of this cost over the 50 runs, for each value of N, is presented in the top part of Fig. 13. The error bars denote the 95% confidence intervals for the computed mean values. The top-left curve corresponding to the SNR = 2.17 dB case displays its minimum at $N = 5$. This behavior indicates that the average optimal MDL reconstruction uses 5 sides at this noise level. A corresponding typical such 5-sided reconstruction of the ellipse is displayed on the lower left plot of Fig. 13 together with the true ellipse. The upper-right curve corresponding to the SNR = 0 dB case displays its minimum at $N = 6$, which indicates that the average optimal MDL reconstruction for this case uses 6 sides. The MDL cost curve for this lower SNR case has now become quite flat however, showing that the reconstruction with N from 4 to 6 are all about equally explanatory of the data. Although the curves for both cases demonstrate the ability of the MDL procedure to capture the shape's complexity through its choice of N, this behavior suggests that with increasing noise intensity, an MDL-based estimate becomes less sensitive to the *precise level* of complexity of the reconstruction, as we would expect. Apparently, in high noise situations the differences between these reconstructions that would be apparent in high SNR scenarios are masked. As the noise level increases, these fine distinctions are unimportant or *not supported by the data*. A typical 6-sided reconstruction is also displayed in the lower right plot of Fig. 13 along with the true ellipse.

As another example of the use of the proposed algorithms, we choose an object that is *nonpolygonal* and *nonconvex*. In Fig. 14, reconstructions of this object are shown based on 20 equally spaced projections with 50 samples per projection, at a signal-to-noise ratio of 4.35 dB. In these reconstructions, a slight variant of the initial

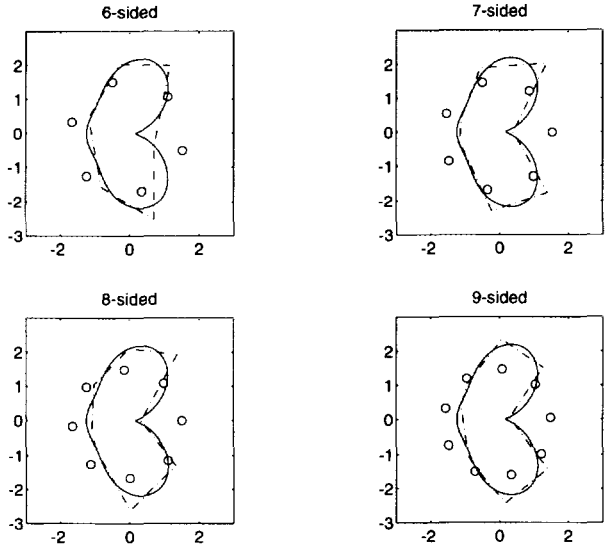

FIG. 14. True object (—), reconstruction (-·), and initial guess (○) picked using the Initial Guess Algorithm; SNR = 4.35 dB.

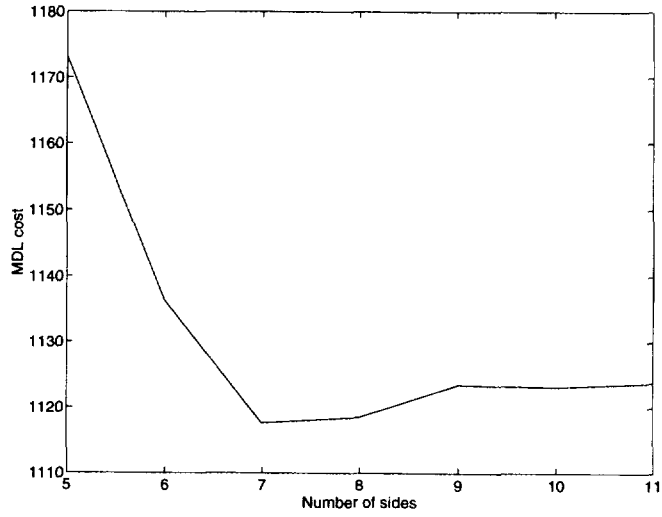

FIG. 16. MDL cost curve for the reconstruction of the kidney-shaped object with the Initial Guess Algorithm used.

guess algorithm was used to generate the starting polygons as we will describe shortly. Figure 15, meanwhile, contains the reconstruction produced by FBP using the same data set. As can be seen, when using 7 or more sides, the underlying object can be captured more accurately and without spurious features through the use of our algorithm.

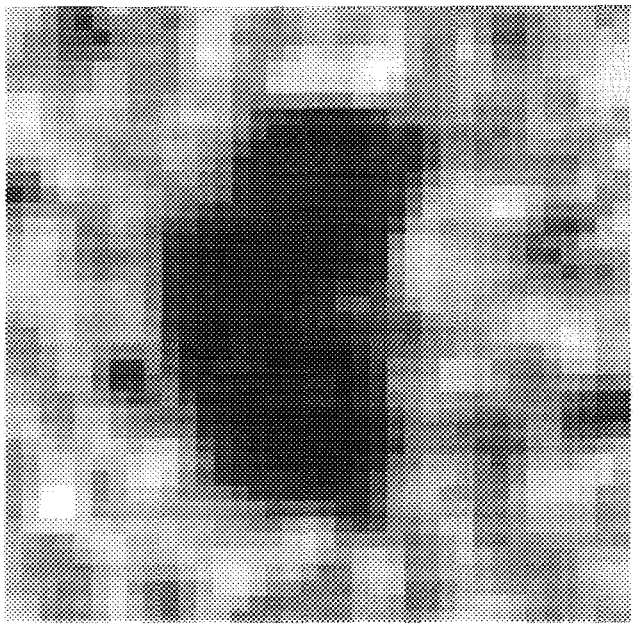

FIG. 15. FBP reconstruction of nonpolygonal, nonconvex object: third-order Butterworth filter with 0.15 normalized cut-off frequency; SNR = 4.35 dB.

To pick the "best" number of sides, in Fig. 16 we show the MDL cost curve for the reconstructions of the kidney-shaped object at SNR = 4.35 dB shown in Fig. 14. In applying our algorithm to this *nonconvex* object, we found that we can improve the resulting reconstructions by slightly perturbing the initialization produced by the proposed Initial Guess Algorithm by rotations through small angles. In particular, recall that according to Result 1, any orthogonal transformation of the initial polygon V_{init} produced by the Initial Guess Algorithm is a "valid" starting guess in the sense that it will have the same first three moments as V_{init}. Taking advantage of this property, for a given number of sides, we applied several small rotations to the V_{init} produced by the Initial Guess Algorithm and carried out the ML optimization problem with these resulting initializations. We then picked the solutions which resulted in the lowest ML cost. Using this procedure for each number of sides, we calculated the MDL cost values shown in Fig. 16. These "best" reconstructions are shown in Fig. 14.[4] We note that, according to Fig. 16, the minimum of the MDL cost corresponds to a reconstruction with 7 sides. As is apparent in Fig. 14, while using a higher number of vertices beyond 7 does improve the reconstructions somewhat, it does not yield significantly better results. This fact is directly reflected in the MDL cost curve becoming increasingly flat beyond 7 sides.

[4] The process of applying an orthogonal transformation to the output of the Initial Guess Algorithm, before using this in the reconstruction algorithm, is one that can perhaps be applied in general. However, we found this modification to be needed only when rather complex, nonconvex and nonpolygonal objects were being reconstructed.

3.4. Initial Guess Algorithm

In this section, we present some sample reconstructions and performance plots for which we use the Initial Guess Algorithm for generating a starting point to the nonlinear optimization (3). These experiments aim to show that the Initial Guess Algorithm does indeed provide us with a starting guess that in the great majority of the cases is near the global optimum. This will, of course, not guarantee convergence to the global optimum solution, but as we shall see, the use of the Initial Guess Algorithm does at least result in convergence to a local minimum of the cost which is almost always quite near the global optimum.

To study the average performance of the ML algorithm using the output of the Initial Guess Algorithm, a Monte Carlo simulation was done for the reconstruction of the hexagon shown in Fig. 5; 100 reconstructions were carried out for different realizations of the noise at various SNRs, each with 1000 projection samples as before (50 projections and 20 samples per projection). For each SNR, on average less than 5% of the reconstructions (i.e., 5 out of 100 sample reconstructions) had very large reconstruction errors (we call these instances *outliers*). Fig. 17 shows the reconstruction errors for 100 realizations of the noise at 0 dB. The outliers are clearly visible.

Figure 17 indicates that in a few instances, the reconstructions were essentially at local minima very far from the global minimum of the cost. In our experience, these outliers occur most frequently when poor estimates of the moments of order 2 are obtained from the noisy data. Note that the second-order moments are used in the Initial Guess Algorithm only if the corresponding inertia matrix obtained from them is strictly positive definite. The Initial Guess Algorithm decides whether to use the second-order moments or not solely on the basis of this positive definiteness and regardless of how close the inertia matrix may be to negative—or indefiniteness. Hence, the outliers occur in those rare instances when the estimated inertia matrix happens to be a very poor estimate, but yet positive definite (and hence used in the Initial Guess Algorithm). This phenomenon, in turn, seems to occur when relatively few samples per projection are available.

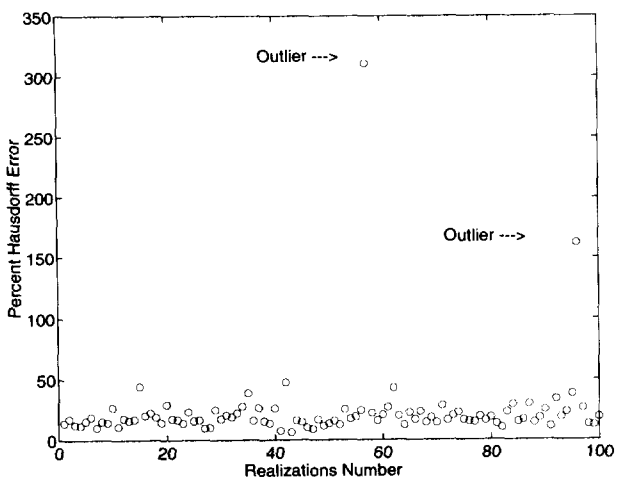

FIG. 17. A sample path of the reconstruction error at SNR = 0 dB.

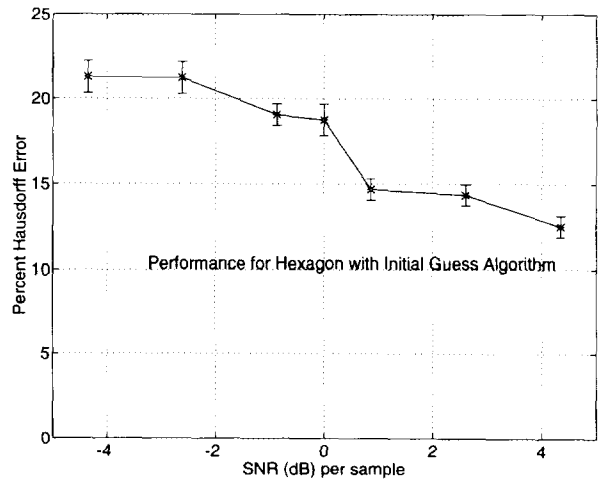

FIG. 18. Percent error for hexagon vs SNR after outlier removal.

Figure 18 shows the mean percent error in the Monte Carlo runs after the removal of the outliers. The outliers were removed from the ensemble and the results of the remaining realizations were averaged to yield the values in Fig. 18. That is to say, that if 3 out of 100 realizations led to outliers, then only those 97 results which seemed "reasonable" were used in computing the ensemble average. Whether the result of a run was deemed reasonable or not was decided by comparing the resulting percent error to the ensemble median reconstruction error for all 100 runs. In particular, if the percent error for a run was larger than one standard deviation away from the *median*, the run was declared an outlier. In the case of Fig. 17, using the computed median value of 17.2 and standard deviation of 33.2, a threshold level of 50.4 was chosen above which outliers were declared.

The resulting "mean" performance is plotted here to show the average performance without the effect of the outliers. It can be seen, upon comparing Fig. 18 with the corresponding performance curve in Fig. 9 that the performance of the ML algorithm using the output of the Initial Guess Algorithm still suffers even after discounting the obvious outliers. This means that instances of convergence to local minima still occur, but note that, at least from a visual standpoint, the average performance after the removal of outliers is not significantly different from the average performance with the actual polygon as the initial guess. In particular, the degradation in performance

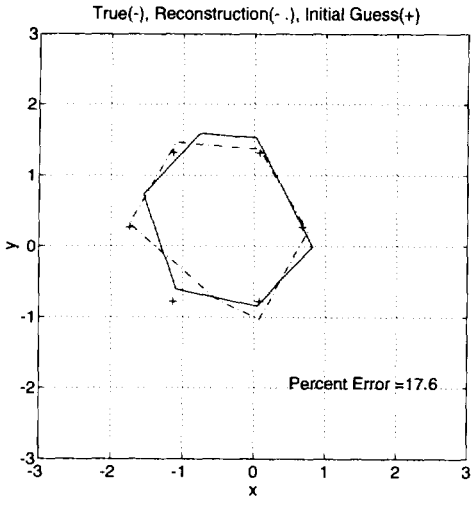

FIG. 19. A typical reconstruction at a local minimum with SNR = 0 dB: true (—), reconstruction (--), and initial guess (+).

here is roughly 7 percentage points in the Hausdorff norm over the given SNR range. This corresponds to a small *visual* error as can be seen in Fig. 4. From this observation, we conclude that even though the Initial Guess Algorithm does not always lead to convergence to the global minimum, it almost always leads to, at least, a local minimum that is fairly close to the global minimum of the cost function. Typical reconstruction at local minima which are close to the global minimum of the cost are shown in Fig. 19 for SNR = 0 dB and in Fig. 20 for SNR = 4.35 dB.

4. CONCLUSIONS

In this paper, we studied statistical techniques for the reconstruction of binary polygonal objects. In particular, we focused on the reconstruction of binary polygonal objects. The reconstruction of such objects was posed as a parameter estimation problem for which the maximum likelihood technique was proposed as a solution. In contrast to the classical techniques, such as FBP, the ML-based reconstructions showed great robustness to noise and data loss and distribution when a good initial guess was available. The drawback of such ML-based formulations is that the resulting optimization problems are highly nonlinear, and thus a good initial guess is necessary to ensure convergence of optimization routines to a solution that is at least near the true ML estimate. To this end, an algorithm was presented for computing such a reasonable initial guess using moments of the object which are estimated directly from the projection data. While estimation of a function from its moments is, in general, a difficult and ill-posed problem, we avoid these problems by using the noisy estimated moments only to guide a coarse object estimate. This estimate, in turn, mitigates the difficulties associated with the nonlinearities of the optimal ML statistical approach. The efficacy of this moment based initial guess algorithm was demonstrated over a range of SNRs.

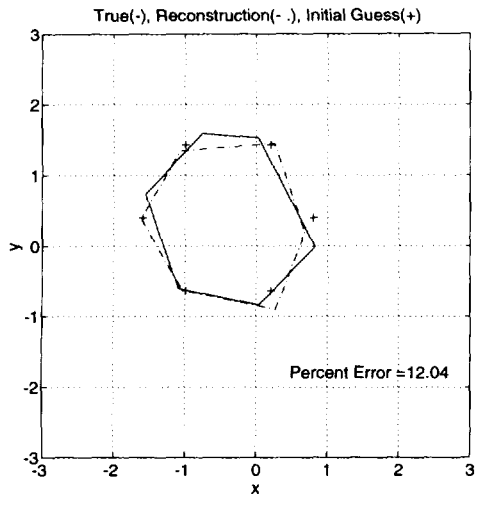

FIG. 20. A typical reconstruction at a local minimum with SNR = 4.35 dB. Symbols as in Fig. 19.

If the number of parameters describing the underlying object are not known, a minimum description length criterion can be employed that simply generalizes the ML framework to penalize the use of an excessively large number of parameters for the reconstruction. The MDL approach was shown to work successfully in estimating the number of sides and the underlying object itself for low signal-to-noise ratio situations and for a variety of sampling scenarios. It was further demonstrated that if the underlying object is not polygonal, but still binary, the proposed ML and MDL algorithms are still capable of producing polygonal reconstructions which reasonably capture the object shape in the presence of high noise intensity.

In this work, we have focused on the reconstruction of binary polygonal objects parameterized by their vertices. The ML- and MDL-based techniques used here may also be applied to more general object parameterizations. In particular, while we used the (estimated) moments of the object only as the basis for generating an initial guess, it is, in some cases, possible to actually parameterize the object entirely through its moments. For instance, Davis [35] has shown that a triangle in the plane is uniquely determined by its moments up to order 3, while in [27, 33] we have generalized this result to show that the vertices of any simply connected nondegenerate N-gon are uniquely determined by its moments up to order $2N - 3$.

More generally, a square integrable function defined over a compact region of the plane is completely determined by the entire set of its moments [28, 29, 31]. In reality, we will only have access to a finite set of these moments, and these numbers, coming from estimates,

will themselves be inexact and noisy. While estimation of the moments of a function based on its projections is a convenient linear problem, inversion of the resulting finite set of moments to obtain the underlying function estimate is a difficult and ill-posed problem. These observations suggest a spectrum of ways in which to use moments in our reconstruction problems. At one extreme, only a few moments are used in a suboptimal way to generate a simple initialization for solution of a hard, nonlinear estimation problem. At the other extreme, the moments are themselves used in an optimal reconstruction scheme. In [26, 27], we have studied regularized variational formulations for the reconstruction of a square integrable function from noisy estimates of a finite number of its moments. We have also studied [33] array-processing-based algorithms for the reconstruction of binary polygonal objects from a finite number of their moments.

APPENDIX A: THEORETICAL RESULTS ON THE INITIAL GUESS ALGORITHM

In this section we present some theoretical justification for the initial guess algorithm. To start, we state some elementary properties of unit area polygons $V_{\text{ref}}(N)$ whose vertices are the scaled Nth roots of unity (in a counterclockwise direction) as defined by (18). From [27], it is a matter of some algebraic manipulations to show that the regular polygon $V_{\text{ref}}(N)$ has moments of up to order 2 given by

$$\mu_{00}(V_{\text{ref}}(N)) = 1 \tag{46}$$

$$\mu_{10}(V_{\text{ref}}(N)) = \mu_{01}(V_{\text{ref}}(N)) = 0 \tag{47}$$

$$\mu_{20}(V_{\text{ref}}(N)) = \mu_{02}(V_{\text{ref}}(N)) = \frac{1}{4N\tan(\pi/N)} = k_N \tag{48}$$

$$\mu_{11}(V_{\text{ref}}(N)) = 0. \tag{49}$$

Now let V_{init} be an affine transformation of V_{ref} as

$$V_{\text{init}} = LV_{\text{ref}}(N) + [C\,|\,C\,|\cdots|\,C] \tag{50}$$

for some linear transformation L and some 2×1 vector C. Let $\mathcal{O}(V_{\text{init}})$ denote the closed, binary polygonal region enclosed by the N-gon V_{init}. Now by considering the change of variables $\mathbf{z} = L\mathbf{u}$, and dropping the explicit dependences on N we have

$$\mu_{00}(V_{\text{init}}) = \int\int_{\mathcal{O}(V_{\text{init}})} d\mathbf{z}, \tag{51}$$

$$= \int\int_{\mathcal{O}(V_{\text{ref}})} |\det(L)|\, d\mathbf{u}, \tag{52}$$

$$= \mu_{00}(V_{\text{ref}})|\det(L)| = |\det(L)|. \tag{53}$$

Similarly, we get

$$[\mu_{10}(V_{\text{init}})\ \mu_{01}(V_{\text{init}})]^{\mathrm{T}} = (L[\mu_{10}(V_{\text{ref}})\ \mu_{01}(V_{\text{ref}})]^{\mathrm{T}} + C)|\det(L)| = |\det(L)|C \tag{54}$$

and

$$\mathcal{I}(V_{\text{init}}) = (L\mathcal{I}(V_{\text{ref}})L^{\mathrm{T}} + CC^{\mathrm{T}})|\det(L)| = (k_N LL^{\mathrm{T}} + CC^{\mathrm{T}})|\det(L)| \tag{55}$$

where for any N-gon V we write

$$\mathcal{I}(V) = \begin{bmatrix} \mu_{20}(V) & \mu_{11}(V) \\ \mu_{11}(V) & \mu_{02}(V) \end{bmatrix}. \tag{56}$$

This proves relations (21), (22), and (23).

We next establish an explicit description of the set of all affinely regular N-gons with a fixed set of moments up to order 2. In order to do this, we first need to prove a lemma.

LEMMA 1. *For every N-gon V with moments μ_{00}, $\mu_{10} = 0$, $\mu_{01} = 0$, μ_{20}, μ_{11}, μ_{02}, such that the inertia matrix $\mathcal{I}$ satisfies $\det(\mathcal{I}) = k_N^2\mu_{00}^4$, there exists a matrix L, unique up to some orthogonal transformation, such that $V = LV_{\text{ref}}$.*

Proof. The assumptions that $\mu_{10} = 0$ and $\mu_{01} = 0$ are made without loss of generality and to facilitate the presentation of the proof. Having said this, we define L as the scaled (unique) square root of $\mathcal{I}$ as follows. First, write the following eigendecomposition

$$\frac{\mathcal{I}}{\sqrt{\det(\mathcal{I})}} = US^2U^{\mathrm{T}}, \tag{57}$$

where U is orthogonal and S has unit determinant. Define L as

$$L = \sqrt{\mu_{00}}US. \tag{58}$$

The moments of $V = LV_{\text{ref}}$ are then given by

$$\mu_{00}(V) = \mu_{00} \tag{59}$$

$$\mu_{10}(V) = \mu_{01}(V) = 0 \tag{60}$$

$$\mathcal{I}(V) = k_N LL^{\mathrm{T}}|\det(L)|. \tag{61}$$

Note that

$$\det(\mathcal{I}) = k_N^2\mu_{00}^4 \tag{62}$$

as required. If L is replaced by LT where T is any 2×2 orthogonal transformation, the same moments are obtained. Hence the lemma is established. ∎

Given this lemma, we obtain an interesting geometric representation of all affinely regular N-gons that have a prespecified set of moments of up to order 2. This characterization is given by Result 1, which we prove next.

Proof of Result 1. For the sake of simplicity, and without loss of generality, we carry out the proof for the case where all polygons are centered at the origin.
Let S_1 denote the set of all N-gons whose first three moment sets are μ_{00}, $\mu_{10} = \mu_{01} = 0$, μ_{20}, μ_{11}, μ_{02}. Let S_2 denote the set of all N-gons with vertices on the ellipse $\mathbf{z}^T E_O^{-1}\mathbf{z} = 1$, and sides tangent (at their midpoints) to the ellipse $\mathbf{z}^T E_I^{-1}\mathbf{z} = 1$. We show that $S_1 = S_2$.

First, consider an N-gon $V \in S_1$. V has moments μ_{00}, 0, 0, $\mathcal{I}$ and therefore, by Lemma 1, there exists an L given by (57) and (58), unique up to some orthogonal matrix T_1 such that we can write

$$V = (LT_1)V_{\text{ref}}(N) \tag{63}$$

Let us denote the N-gons V and $V_{\text{ref}}(N)$ explicitly in terms of their columns as

$$V = [v_1 | v_2 | \cdots | v_N] \tag{64}$$

$$V_{\text{ref}}(N) = [w_1 | w_2 | \cdots | w_N] \tag{65}$$

so that

$$v_j = LT_1 w_j. \tag{66}$$

It is easy to show from the definition of $V_{\text{ref}}(N)$ that

$$w_j^T w_j = \alpha_N = \frac{1}{(N/2)\sin(2\pi/N)}, \tag{67}$$

$$(w_{j+1} + w_j)^T(w_{j+1} + w_j) = 4\beta_N = \frac{4}{N\tan(\pi/N)}. \tag{68}$$

Now to show that $V \in S_2$, we prove that

$$v_j^T E_O^{-1} v_j = 1 \tag{69}$$

$$\frac{(v_{j+1} + v_j)^T}{2} E_I^{-1} \frac{(v_{j+1} + v_j)}{2} = 1 \tag{70}$$

for $j = 1, 2 \cdots N$, where by convention, $N + 1 = 1$. Using (57) and (58), we can write

$$v_j^T E_O^{-1} v_j = \frac{\mu_{00} k_N}{\alpha_N} v_j^T \mathcal{I}^{-1} v_j. \tag{71}$$

$$= \frac{\mu_{00} k_N}{\alpha_N} \frac{1}{k_N \mu_{00}^2} \mu_{00} w_j^T T_1^T S U^T U S^{-2} U^T U S T_1 w_j. \tag{72}$$

$$= \frac{1}{\alpha_N} w_j^T w_j. \tag{73}$$

$$= 1. \tag{74}$$

Similarly,

$$\frac{(v_{j+1} + v_j)^T}{2} E_I^{-1} \frac{(v_{j+1} + v_j)}{2}$$

$$= \frac{1}{4} \frac{\mu_{00} k_N}{\beta_N} \frac{1}{k_N \mu_{00}^2} \mu_{00} (v_{j+1} + v_j)^T \mathcal{I}^{-1} (v_{j+1} + v_j)$$

$$= \frac{1}{4\beta_N} (w_{j+1} + w_j)^T (w_{j+1} + w_j) \tag{75}$$

$$= 1. \tag{76}$$

Hence, $V \in S_2$.

Now assume that $V \in S_2$. Then, by assumption,

$$v_j^T E_O^{-1} v_j = 1 \tag{77}$$

$$\frac{(v_{j+1} + v_j)^T}{2} E_I^{-1} \frac{(v_{j+1} + v_j)}{2} = 1. \tag{78}$$

Define the vertices of the related N-gon Z as

$$z_j = \frac{1}{\sqrt{\alpha_N \mu_{00}}} S^{-1} U^T v_j, \tag{79}$$

where S and U are given by the normalized eigendecomposition of $\mathcal{I}$ given in (57). Writing (77) and (78) in terms of z_j, after some algebraic manipulations, we get

$$z_j^T z_j = 1 \tag{80}$$

$$\frac{(z_{j+1} + z_j)^T}{2} \frac{(z_{j+1} + z_j)}{2} = \cos^2\left(\frac{\pi}{N}\right). \tag{81}$$

From these identities, again with some algebraic manipulation, it easily follows that Z is equilateral. Specifically,

$$\|z_{j+1} - z_j\|^{1/2} = 2\sin\left(\frac{\pi}{N}\right). \tag{82}$$

Since the above identities show that the N-gon Z is a regular N-gon inscribed in the unit circle, then it must be related to $V_{\text{ref}}(N)$ through a scaling and some orthogonal transformation T_2. In particular,

$$Z = \sqrt{\frac{N}{2}\sin\left(\frac{2\pi}{N}\right)}\, T_2 V_{\text{ref}}(N) \tag{83}$$

This in turn shows that

$$\frac{1}{\sqrt{\alpha_N \mu_{00}}} S^{-1} U^T V = \sqrt{\frac{N}{2} \sin\left(\frac{2\pi}{N}\right)}\, T_2 V_{\text{ref}}(N), \quad (84)$$

or, after solving for V and simplifying,

$$V = \sqrt{\mu_{00}}\, U S T_2 V_{\text{ref}}(N). \quad (85)$$

Letting $L = \sqrt{\mu_{00}}\, US$, we obtain

$$V = (LT_2) V_{\text{ref}}(N). \quad (86)$$

This last identity implies that V has moments $\mu_{00}(V) = \mu_{00}$, $\mu_{10}(V) = \mu_{01}(V) = 0$, and

$$\mathcal{I}(V) = k_N L L^T |\det(L)| \quad (87)$$

with $\det(\mathcal{I}(V)) = k_N^2 \mu_{00}^4$. Hence $V \in S_1$ and the result is established. ■

If $\mathcal{I}$ is not the inertia matrix of an affinely regular N-gon then the L constructed in the Initial Guess Algorithm will not have the prescribed inertia matrix. We are, however, able to explicitly compute the approximation error in the following way.

RESULT 2. *Suppose that the moments* μ_{00}, $\mu_{10} = \mu_{01} = 0$,

$$\mathcal{I} = \begin{bmatrix} \mu_{20} & \mu_{11} \\ \mu_{11} & \mu_{02} \end{bmatrix} \quad (88)$$

are given such that $\det(\mathcal{I}) = k_N^2 \mu_{00}^4 + \varepsilon > 0$. *Define*

$$L = \sqrt{\mu_{00}}\, US, \quad (89)$$

where

$$\frac{\mathcal{I}}{\sqrt{\det(\mathcal{I})}} = US^2U^T \quad (90)$$

is the normalized eigendecomposition of $\mathcal{I}$. *Then the normalized Frobenius-norm error is given by*

$$\frac{\|\mu_{00} k_N L L^T - \mathcal{I}\|_F}{\|\mathcal{I}\|_F} = \left| 1 - \frac{k_N \mu_{00}^2}{\sqrt{k_N^2 \mu_{00}^4 + \varepsilon}} \right|. \quad (91)$$

Proof. Letting $A = \mu_{00} k_N L L^T$ and $B = \mathcal{I}$, we can write

$$A = aUS^2U^T, \quad (92)$$

$$B = bUS^2U^T, \quad (93)$$

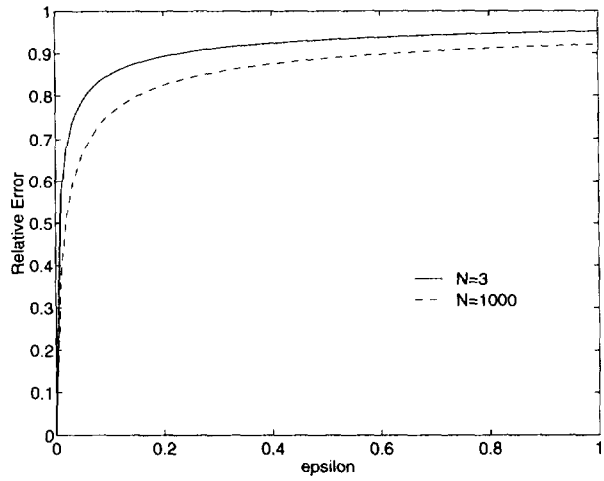

FIG. 21. Relative error in matching second order moments using the Initial Guess Algorithm.

where

$$S^2 = \begin{bmatrix} \lambda & 0 \\ 0 & 1/\lambda \end{bmatrix}, \quad (94)$$

$$a = k_N \mu_{00}^2, \quad (95)$$

$$b = \sqrt{k_N^2 \mu_{00}^4 + \varepsilon}. \quad (96)$$

Hence, we have

$$\|A - B\|_F = \|(a - b)S^2\|_F = |a - b| \sqrt{\lambda^2 + \frac{1}{\lambda^2}}, \quad (97)$$

$$\|B\|_F = |b| \sqrt{\lambda^2 + \frac{1}{\lambda^2}}. \quad (98)$$

Hence,

$$\frac{\|A - B\|_F}{\|B\|_F} = \frac{|a - b|}{|b|} = \frac{|\sqrt{k_N^2 \mu_{00}^4 + \varepsilon} - k_N \mu_{00}^2|}{\sqrt{k_N^2 \mu_{00}^4 + \varepsilon}} = \left| 1 - \frac{k_N \mu_{00}^2}{\sqrt{k_N^2 \mu_{00}^4 + \varepsilon}} \right| \quad (99)$$

which establishes the result. ■

We have plotted the expression for the relative error in Fig. 21 for $N = 3$ and $N = 1000$, assuming that $\mu_{00} = 1$. This figure shows that although the relative error grows quite fast as ε increases, it never exceeds the maximum of 1 (i.e., 100%) for a fixed μ_{00}. Also, the relative errors for different number of sides are seen to be very close.

ACKNOWLEDGMENTS

The authors wish to acknowledge the anonymous reviewers for their extremely constructive and useful suggestions.

REFERENCES

1. M. Bergstrom, J. Litton, L. Ericksson, C. Bohm, and G. Blomqvist, Determination of object contour from projections for attenuation correction in cranial positron emission tomography, *J. Comput. Assist. Tomography* **6,** 1982, 365–372.
2. J.-P. Thirion, Segmentation of tomographic data without image reconstruction, *IEEE Trans. Med. Imaging* **11,** Mar. 1992, 102–110.
3. N. Srinivasa, K. Ramakrishnan, and K. Rajgopal, Detection of edges from projections, *IEEE Trans. Med. Imaging* **11,** Mar. 1992, 76–80.
4. W. Munk and C. Wunsch, Ocean acoustic tomography: a scheme for larger scale monitoring, *Deep-Sea Res.* **26A,** 1979, 123–161.
5. G. T. Herman, *Image Reconstruction From Projections*, Academic Press, New York, 1980.
6. D. Rossi and A. Willsky, Reconstruction from projections based on detection and estimation of objects—parts I and II: Performance analysis and robustness analysis, *IEEE Trans. Acoust. Speech Signal Process.* **32,** Aug. 1984, 886–906.
7. J. L. Price and A. S. Willsky, Estimating convex sets from noisy support line measurements, *IEEE Trans. Pattern Anal. Mach. Intell.* **12,** 1990, 377–389.
8. J. L. Prince and A. S. Willsky, A geometric projection-space reconstruction algorithm, *Linear Algebra Appl.* **130,** 1990, 151–191.
9. J. L. Prince, *Geometric Model-Based Estimation from Projections*, Ph.D. thesis, Dept. of EECS, MIT, 1988.
10. A. Lele, S. Kulkarni, and A. Willsky, Convex-polygon estimation from support-line measurements and applications to target reconstruction from laser-radar data, *J. Opt. Soc. Am.* **9,** Oct. 1992, 1693–1714.
11. A. Lele, *Convex Set Estimation from Support Line Measurements*, Master's thesis, Dept. of EECS, MIT, 1990.
12. K. Hanson, Tomographic reconstruction of axially symmetric objects from a single radiograph, in *High Speed Photography*, Videography and Photonics, No. II (A. L. Vick, Ed.), Proceedings of SPIE, Vol. 491, SPIE, Bellingham, WA, 1984.
13. W. C. Karl, *Reconstructing Objects from Projections*, Ph.D. thesis, Dept. of EECS, MIT, 1991.
14. Y. Bresler and A. Macovski, Estimation of 3-d shape of blood vessels from X-ray images, in *Proc. IEEE Int. Conf. on Acoustics, Speech and Signal Processing, March 1984.*
15. Y. Bresler, J. Fessler, and A. Macovski, A bayesian approach to reconstruction from incomplete projections of a multiple object 3D domain, *IEEE Trans. Pattern Anal. Mach. Intell.* **11,** Aug. 1989, 840–858.
16. Y. Bresler and A. Macovski, Three-dimensional reconstruction from projections with incomplete and noisy data by object estimation, *IEEE Trans. Acoust. Speech Signal Process.* **ASSP-35,** Aug. 1987, 1139–1152.
17. J. A. Fessler and A. Macovski, Object-based 3-d reconstruction of arterial trees from magnetic resonance angiograms, *IEEE Trans. Med. Imaging* **10,** Mar. 1991, 25–39.
18. S. Chang, The reconstruction of binary patterns from their projections, *Comm. ACM* **14**(1), 1971.
19. A. Kuba, Reconstruction of measurable plane sets from their two projections taken in arbitrary directions, *Inverse Problems* **7,** 1991, 101–107.
20. A. Volcic, A three point solution to Hammer's X-ray problem, *J. London Math. Soc.* **2**(34), 1986, 349–359.
21. P. C. Fishburn, J. Lagarias, J. Reeds, and L. A. Shepp, Sets uniquely determined by projections on axes I. Continuous case, *SIAM J. Appl. Math.* **50**(1), 1990, 288–306.
22. R. J. Gardner, Symmetrals and X-rays of planar convex bodies, *Arch. Math.* **41,** 1983, 183–189.
23. S. Helgason, *Radon Transform*, Birkhauser, Boston, 1980.
24. H. VanTrees, *Detection, Estimation, and Modulation Theory: Part I*, Wiley, New York, 1968.
25. J. Rissanen, *Stochastic Complexity in Statistical Inquiry*, Series in Computer Science, Vol. 15, World Scientific, Singapore, 1989.
26. P. Milanfar, W. C. Karl, and A. S. Willsky, A moment-based variational approach to tomographic reconstruction, submitted for publication.
27. P. Milanfar, *Geometric Estimation and Reconstruction from Tomographic Data*, Ph.D. thesis, Department of EECS, MIT, June 1993.
28. G. Talenti, Recovering a function from a finite number of moments, *Inverse Problems* **3,** 1987, 501–517.
29. J. Shohat and J. Tamarkin, *The Problem of Moments*, American Mathematical Society, New York, 1943.
30. M. Pawlak, On the reconstruction aspects of moments descriptors, *IEEE Trans. Inform. Theory* **38,** Nov. 1992, 1698–1708.
31. N. Akhiezer, *The Classical Moment Problem and Some Related Questions in Analysis*, Hafner, New York, 1965.
32. M. Berger, *Geometry I and II*, Springer-Verlag, Berlin/New York, 1987.
33. P. Milanfar, G. C. Verghese, W. C. Karl, and A. S. Willsky, Reconstructing polygons from moments with connections to array processing, *IEEE Trans. Signal Process.*, Feb. 1994, to appear.
34. J. Nelder and R. Mead, A simplex method for function minimization, *Computer J.* **7,** 1970, 308–313.
35. P. J. Davis, Plane regions determined by complex moments, *J. Approx. Theory* **19,** 1977, 148–153.